Continuum Modeling of Bulk Metallic Glasses and Composites

Fadi Abdeljawad*
Department of Mechanical and Aerospace Engineering, Princeton University, Princeton, New Jersey 08544, USA

Mikko Haataja†
Department of Mechanical and Aerospace Engineering, Princeton Institute for the Science and Technology of Materials (PRISM), and Program in Applied and Computational Mathematics (PACM), Princeton University, Princeton, New Jersey 08544, USA
(Received 29 April 2010; published 17 September 2010)

At low temperatures, monolithic bulk metallic glasses (BMGs) exhibit high strength and large elasticity limits. On the other hand, BMGs lack overall ductility due to highly localized deformation mechanisms. Recent experimental findings suggest that the problem of catastrophic failure by shear band propagation in BMGs can be mitigated by tailoring microstructural features at different length scales to promote more homogeneous plastic deformation. Herein, based on a continuum approach, we present a quantitative analysis of the effects of microstructure on the deformation behavior of monolithic BMGs and BMG composites. In particular, simulations highlight the importance of short-ranged structural correlations on ductility in monolithic BMGs and demonstrate that particle size controls the ductility of BMG composites. In broader terms, our results provide new avenues for further improvements to the mechanical properties of BMGs.

DOI: 10.1103/PhysRevLett.105.125503 PACS numbers: 62.20.F−, 81.05.Kf

Monolithic bulk metallic glasses (BMGs) appear macroscopically homogeneous, yet contain structural and chemical heterogeneities at the atomic scale [1–5]. They are characterized by their near theoretical strength and large elasticity limit [6,7]. However, BMGs exhibit a limited amount of *global* plasticity. Plastic flow in such featureless structures typically becomes highly localized in shear bands, and catastrophic failure subsequently occurs by shear softening on one band [7,8].

In general, the overall ductility of BMG systems can be improved by either fine-tuning the alloy composition of monolithic BMGs or by introducing ductile particles into the glassy matrix, thus forming a BMG composite. In the former case, variations in the critical shear stress were proposed to correlate with the degree of short- (SRO) and medium-range order [4,5]. Experimental and computational analysis of model BMGs revealed that SRO is associated with solute-centered polyhedra with varying atomic coordination numbers and resistance to slip; these polyhedra subsequently pack together to fill three-dimensional space, giving rise to medium-range order [9–11]. Atomistic simulations of monolithic BMGs have shown that deformation changes from homogeneous flow, with improved ductility, to a more localized state as the fraction of atoms exhibiting SRO increases [12,13].

In the latter case, enhanced overall ductility in several BMG systems has been achieved by introducing ductile crystalline dendrites with size scales 1–100 μm, resulting in BMG composites [14–19]. Ductile dendrites can act both as shear band initiation sites and as arrest barriers to shear band extension [14,15]. Shear band branching leads to a more uniform distribution of plastic strain, and the result is a BMG composite whose properties can be optimized with respect to morphology and volume fraction of the ductile phase [14]. For example, it was shown in Ref. [19] that the ultimate strain $\gamma_{\mathrm{tot}} \approx w_{\mathrm{SB}}/\lambda$, where w_{SB} and λ denote shear band thickness and spacing, respectively, while λ was found to correlate with the dendritic secondary arm spacing. These observations thus suggest that overall ductility can be improved by decreasing shear band spacing by appropriately tailoring the microstructure.

Given that both of the aforementioned routes to improving ductility of BMGs are associated with tailoring microstructural features, albeit at different length scales, it would be highly advantageous to have a computationally tractable, multiscale description of deformation phenomena in BMG systems. Existing theoretical approaches focus on either atomistic properties of BMG composites [20–22], which are computationally difficult to scale up to the meso- and macroscales, or mesoscale properties of monolithic BMGs; the latter approach usually incorporates coarse-grained shear transformation zones as the main carriers of plasticity [23–30]. In this Letter, we present a diffuse-interface model, which phenomenologically incorporates the spatial heterogeneity of metallic glasses at the atomic scale and captures the formation and propagation of shear bands and their interaction with ductile particles at larger length scales. By using this approach, we demonstrate that the connectivity of rigid SRO regions plays a key role in the deformation behavior of monolithic BMGs, while in the BMG composite case, we quantify the effects of ductile particle size and area fraction on ductility.

The theory may be developed as follows. As in conventional shear transformation zone approaches, we assume that every volume element in the BMG is susceptible to a localized slip event in a direction dictated by the (unit)

vector $\hat{\mathbf{n}}(\mathbf{r})$; the spatial variation in $\hat{\mathbf{n}}$ reflects the structural heterogeneity in the glass. In the subsequent analysis, we focus on 2D systems; extension to 3D is straightforward. Next, we write down a local nonlinear deformation energy density, which is multivalued in the shear strain along $\hat{\mathbf{n}} = [\cos\theta(\mathbf{r}), \sin\theta(\mathbf{r})]$ (and thus allows for slip events [31]), in terms of the displacement field $\mathbf{u}(\mathbf{r}, t)$:

$$\mathcal{E}(\mathbf{r}) = \frac{K(\mathbf{r})}{2} e_1^2 + \frac{\mu(\mathbf{r})}{2}\left\{e_2^2 + \frac{\Delta^2(\mathbf{r})}{2\pi^2}\left[1 - \cos\left(\frac{2\pi e_3}{\Delta(\mathbf{r})}\right)\right]\right\}. \tag{1}$$

Here, $u_{ij} \equiv \partial u_i/\partial x_j$, $\epsilon_{ij} \equiv (\partial u_i/\partial x_j + \partial u_j/\partial x_i)/2$, $e_1 \equiv u_{xx} + u_{yy}$, $e_2 \equiv (u_{xx} - u_{yy})\cos 2\theta + (u_{xy} + u_{yx})\sin 2\theta$, and $e_3 \equiv (u_{xy} + u_{yx})\cos 2\theta - (u_{xx} - u_{yy})\sin 2\theta$, while $K(\mathbf{r})$ and $\mu(\mathbf{r})$ denote the bulk and shear moduli, respectively, which generally vary within the microstructure and are deformation history-dependent [32,33]. We note that the expression in Eq. (1) reduces to the standard quadratic elastic energy density [34] in the small strain limit.

Under simple shear, active shear transformation zones are oriented such that $\theta = 0$ or $\pi/2$, which implies that the total deformation energy can be written as

$$\mathcal{F} = \int d\mathbf{r}\left(\frac{K(\mathbf{r})}{2}(u_{xx} + u_{yy})^2 + \frac{\mu(\mathbf{r})}{2}\left\{(u_{xx} - u_{yy})^2 + \frac{\Delta^2(\mathbf{r})}{2\pi^2}\left[1 - \cos\left(\frac{2\pi}{\Delta(\mathbf{r})}(u_{xy} + u_{yx})\right)\right]\right\}\right) + \frac{W^2}{2}\int d\mathbf{r}[(\nabla u_{xx})^2 + (\nabla u_{yy})^2 + 4(\nabla \epsilon_{xy})^2]. \tag{2}$$

Here, $\Delta(\mathbf{r})$ can be interpreted in two equivalent ways: It sets the local shear strain that each element has to experience in order to undergo a phase transition between unslipped and slipped states, and it also controls the energy barrier associated with such a slip event. In the crystalline phase $\Delta(\mathbf{r})$ is constant [31], while in the glassy phase structural heterogeneity can be incorporated by assuming that $\Delta(\mathbf{r})$ is a quenched, Gaussian random variable with average $\langle\Delta(\mathbf{r})\rangle = \Delta_0$ and a two-point correlation function $\langle[\Delta(\mathbf{r}) - \Delta_0][\Delta(\mathbf{r}') - \Delta_0]\rangle = \sigma^2 \exp(-|\mathbf{r} - \mathbf{r}'|/\xi)$, where σ^2 and ξ denote the variance of the distribution and a structural correlation length, respectively. In monolithic BMGs, $\Delta(\mathbf{r})$ is used as a descriptor that distinguishes between domains of rigid and soft SRO. Details of how $\Delta(\mathbf{r})$ is used to characterize regions of rigid or soft SRO are discussed below. We note that in the limit $\Delta = \text{const}$, our model reduces to the treatment of plasticity in monolithic BMGs at a mean-field level by Johnson and Samwer [35] with a local strain at the onset of shear banding of $\langle\Delta\rangle_{\text{BMG}}/4$. As is customary in diffuse-interface approaches, the last term in Eq. (2) contains higher order gradients in the displacement field and is invoked to regularize strain gradients on scales $\lesssim W/\sqrt{\mu}$, where W represents an effective interfacial energy. Finally, within the Ginzburg-Landau formalism adopted here, the dynamics of the dimensionless displacement field follow from [31]

$$\frac{\partial^2 u_i}{\partial t^2} - \eta^* \nabla^2 \frac{\partial u_i}{\partial t} = -\Gamma^* \frac{\delta F}{\delta u_i}, \qquad i = x, y, \tag{3}$$

where $\Gamma^* = \frac{t_r^2 K_r}{\rho_0 l_r^2}$ and $\eta^* = \frac{\eta t_r}{\rho_0 l_r^2}$ are dimensionless parameters controlling the elastic wave speed and the damping characteristics of the system, respectively. Here, η and ρ_0 denote shear viscosity and mass density, respectively, while t_r, l_r, and K_r are the reference units for time, length, and stress, respectively. In this work, length scales were measured in terms of the structural correlation length $\xi \sim 1$ nm, while stress components were measured in units of the bulk modulus of the ductile phase. BMG systems were simulated under simple shear with a net macroscopic strain of 18%. The dynamical equations for the displacement field were integrated on a 512×512 uniform lattice with $\Delta x = \Delta y = 1$ and a time step $\Delta t = 0.003$. $\eta^* = 80$ and $\Gamma^* = 240$ and were chosen such that stresses relax effectively instantaneously relative to the externally imposed (dimensionless) strain rate 2×10^{-4} up until the propagation of incipient shear bands.

Let us first examine the effects of rigid or soft SRO distributions on the mechanical behavior of monolithic BMGs, modeled as two-phase microstructures with an area fraction ϕ corresponding to the rigid SRO populations. Regions with full icosahedra are rigid and have higher shear transition barriers [9]; thus, they are assigned larger Δ_0 values than soft SRO domains. In order to assess the role of structural heterogeneities in the deformation behavior of BMGs, Δ_0 values for rigid or soft SRO domains were varied such that the average $\Delta(\mathbf{r})$ for the whole BMG system is fixed at $\langle\Delta(\mathbf{r})\rangle_{\text{BMG}} = 0.6$; in mean-field theory, the total strain at failure is 0.15. The spatial variations in Δ were implemented as follows. First, two representative distributions of rigid and soft SRO, $\Delta_r(\mathbf{r})$ and $\Delta_s(\mathbf{r})$, respectively, were generated with $\sigma^2 = 0.0125$ but differing in Δ_0 as discussed above. Next, a fraction ϕ of the lattice sites were independently labeled as rigid SROs. Once a given lattice site was labeled rigid (soft), its Δ value was set equal to the local Δ_r (Δ_s) value. $K(\mathbf{r}) = \mu(\mathbf{r}) = 2$ [36], while $\xi = 2$ and $W = 1$. Results were averaged over 5 runs to account for sample-to-sample variations.

Several monolithic BMGs were examined, denoted BMG1, BMG2, and BMG3, with $\phi = 0.9$, 0.6, and 0.4, respectively. For these cases, $\Delta_0 = 0.65$, 0.82, and 1.1 ($\Delta_0 = 0.21$, 0.27, and 0.27) in the rigid (soft) regions. In BMG1 and BMG2, rigid SRO regions percolate, while in BMG3, rigid SRO sites form spatially disconnected regions. A representative microstructure and shear strain contours at 8% and 9% nominal strain for BMG1 are shown in Figs. 1(a)–1(c). The nonuniform strain distribution seen in Fig. 2(b) arises from the structural heterogeneity associated with the rigid or soft SRO regions. Above 8.5% nominal strain, the deformation in BMG1 becomes

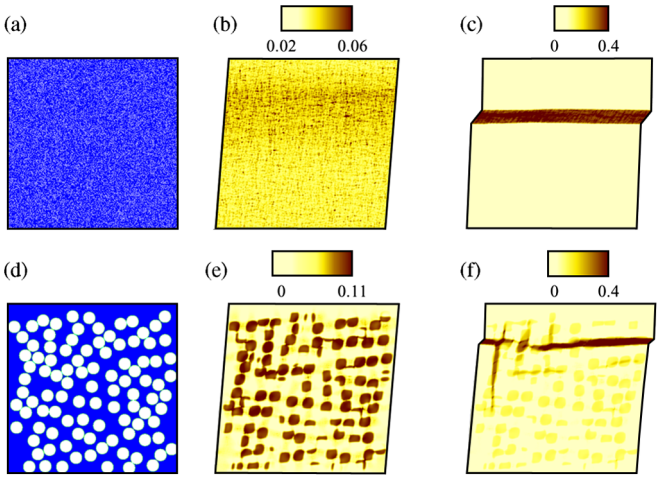

FIG. 1 (color online). (a) Representative microstructure of BMG1, 90% area fraction of rigid SRO. Dark domains represent rigid SRO. Shear strain contours for BMG1 at (b) 8% and (c) 9% nominal strain. A single shear band has formed and propagated through the sample. (d) Representative microstructure of a BMG composite with 40% area fraction of ductile phase and particle size $R = 36.5$. Dark (light) domains represent the glassy (ductile) phases. Shear strain contours for the BMG composite at (e) 8% and (f) 11% nominal strain. Plastic strain accumulates in ductile particles prior to shear banding.

highly localized in a single shear band. Shear stress-strain curves for the three monolithic BMGs are depicted in Fig. 2(a). Ductility is enhanced, while strength is reduced, as ϕ decreases. This trend is in agreement with atomistic simulations of BMGs [9,12]. Note the dramatic deviations of the global strain at the onset of shear banding from the mean-field theory prediction $\langle\Delta\rangle_{\mathrm{BMG}}/4 = 0.15$.

Next we examine the role of ductile domains on the mechanical properties of BMG composites. To this end, composite microstructures were generated by randomly placing circular ductile particles in the glassy matrix. Two BMG composites, each with 40% area fraction of crystalline phase but differing in the particle size R ($R = 36.5$ and $R = 10.5$, respectively), were examined. Figure 1(d) shows a representative BMG composite with particle size $R = 36.5$. The glassy phase was assumed to be rich in rigid SRO with $\langle\Delta(\mathbf{r})\rangle = \Delta_0 = 0.6$, $\xi = 1$, and $\sigma^2 = 0.08$, while for the ductile phase, $\Delta(\mathbf{r}) = 0.2$. $K(\mathbf{r}) = \mu(\mathbf{r}) = 2$ in the glassy phase and were assumed to be twice as large as the moduli for the ductile phase. To account for sample-to-sample variations, results were averaged over 10 runs.

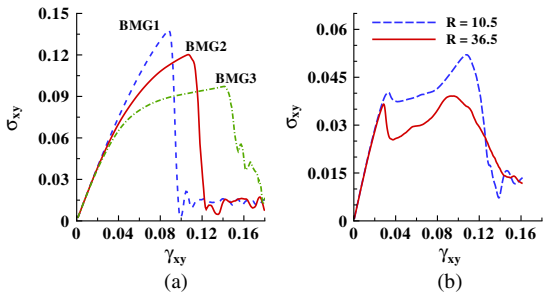

FIG. 2 (color online). Shear stress σ_{xy} vs shear strain γ_{xy} curves for (a) monolithic BMGs (BMG1, BMG2, and BMG3) with area fractions of rigid SRO $\phi = 90\%$, 60%, and 40%, respectively. (b) BMG composites with particle sizes $R = 36.5$ and 10.5 (40% area fraction of ductile phase).

Figures 1(e) and 1(f) show shear strain contours for the BMG composite with $R = 35.6$ at 8% and 11% nominal strains, respectively. The heterogeneous nature of BMG composite microstructure leads to a nonuniform state of deformation, as can be seen in Fig. 1(e). Plastic strain accumulates in the ductile domains due to their low energy barrier to slip. Shear bands develop in the BMG composite at a later stage (11% nominal strain) than the monolithic counterpart (8.5% nominal strain), implying that the addition of ductile particles mitigates shear banding. Figure 2(b) shows stress-strain curves for the BMG composites, which exhibit strain-induced hardening and large plastic strain values. At 40% area fraction of the ductile phase, the BMG composite with smaller particle size ($R = 10.5$) exhibits more ductility and higher strength values than the one with $R = 36.5$. This is due to the presence of glass-crystalline interfaces along with the elastic mismatch, which enable plastic deformation to be globally distributed, thereby mitigating shear band nucleation.

Last, we examine the ultimate strength σ_{UTS} and total strain to failure γ_f (peak point in the stress-strain curve) as a function of morphology and area fraction ϕ of the ductile particles. As depicted in Fig. 3(a), σ_{UTS} of a composite decreases monotonically as the content of the crystalline phase increases. At a fixed ϕ, composites with smaller particles exhibit higher strength values. The trend observed in Fig. 3(a) was experimentally observed in BMG composites, where the compressive or tensile yield strengths are monotonically decreasing functions of the area fraction [14]. Furthermore, Fig. 3(a) also shows the nonlinear behavior of γ_f as a function of ϕ. Small area fractions are

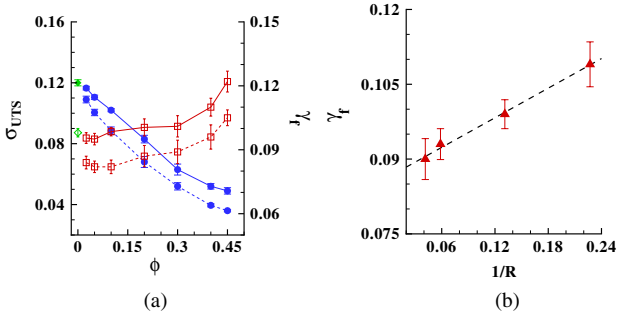

FIG. 3 (color online). (a) Ultimate strength σ_{UTS} (filled symbols) and total strain to failure γ_f (open symbols) for BMG composites with particle sizes $R = 36.5$ (dashed lines) and 10.5 (solid lines). Green symbols correspond to monolithic BMGs. Notice the nonlinear dependence of γ_f on ϕ. (b) Particle size dependence of γ_f at $\phi = 35\%$.

ineffective in improving ductility, while larger area fractions lead to an increase in γ_f over the monolithic BMG. At a fixed ϕ, a large number of small crystalline domains is more effective in obstructing the extension of shear bands than a small number of large domains. At ϕ values above ~40%, ductility increases rapidly for both BMG composites. The nonlinear dependence of γ_f on ϕ can be related to a percolation transition in the BMG composite [14]. Finally, at a fixed ϕ, the data in Fig. 3(b) suggest that $\gamma_f(R) \approx \gamma_f^0 + \text{const}/R$, implying that ductility of BMG composites can be improved by introducing fine-scale microstructural features. These trends in the data can be explained by assuming that the shear band spacing $\lambda \sim R$ and further assuming that the plastic strain $\gamma_f \approx w_{\text{SB}}/\lambda$, in accordance with Ref. [19]. Our findings suggest that, in addition to the volume fraction of the ductile phase, the mechanical properties of BMG systems can be optimized with respect to the characteristic particulate length scales and morphology.

In summary, we have introduced a mesoscale model for BMG systems, which accounts for the structural heterogeneity of glass and captures the fundamental aspects of plastic deformation in such systems. The effect of internal structure, characterized by rigid or soft SRO, on the deformation behavior of monolithic BMGs was investigated, while for BMG composites, we examined the roles of ductile particle size and area fraction in enhancing overall ductility. In the former case, we demonstrated that the connectivity of the rigid SRO regions plays a key role in the deformation behavior of monolithic BMGs, while in the latter case, it was shown that (a) the ductility of the composite is a nonlinear function of ϕ and (b) ductility is inversely proportional to the ductile particle size.

The authors thank Dr. Lisa Manning for stimulating discussions. This work has been in part supported by NSF-DMR Grant No. DMR-0449184.

*fabdelja@princeton.edu
†mhaataja@princeton.edu

[1] J. G. Wang, D. Q. Zhao, M. X. Pan, C. H. Shek, and W. H. Wang, Appl. Phys. Lett. **94**, 031904 (2009).
[2] A. R. Yavari, J. J. Lewandowski, and J. Eckert, MRS Bull. **32**, 635 (2007).
[3] D. B. Miracle, T. Egami, K. M. Flores, and K. F. Kelton, MRS Bull. **32**, 629 (2007).
[4] K. F. Yao, F. Ruan, Y. Q. Tang, and N. Chen, Appl. Phys. Lett. **88**, 122106 (2006).
[5] L. Q. Xing, Y. Li, K. T. Ramesh, J. Li, and T. C. Hufnagel, Phys. Rev. B **64**, 180201 (2001).
[6] M. Chen, Annu. Rev. Mater. Res. **38**, 445 (2008).
[7] C. A. Schuh, T. C. Hufnagel, and U. Ramamurty, Acta Mater. **55**, 4067 (2007).
[8] J. Das, M. B. Tang, K. B. Kim, R. Theissmann, F. Baier, W. H. Wang, and J. Eckert, Phys. Rev. Lett. **94**, 205501 (2005).
[9] L. Zhang, Y. Q. Cheng, A. J. Cao, J. Xu, and E. Ma, Acta Mater. **57**, 1154 (2009).
[10] H. W. Sheng, W. K. Luo, F. M. Alamgir, J. M. Bai, and E. Ma, Nature (London) **439**, 419 (2006).
[11] D. B. Miracle, Nature Mater. **3**, 697 (2004).
[12] Y. Shi and M. L. Falk, Phys. Rev. Lett. **95**, 095502 (2005).
[13] Y. Shi and M. L. Falk, Scr. Mater. **54**, 381 (2006).
[14] M. L. Lee, Y. Li, and C. A. Schuh, Acta Mater. **52**, 4121 (2004).
[15] D. C. Hofmann, J. Y. Suh, A. Wiest, G. Duan, M. L. Lind, M. D. Demetriou, and W. L. Johnson, Nature (London) **451**, 1085 (2008).
[16] M. E. Launey, D. C. Hofmann, W. L. Johnson, and R. O. Ritchie, Proc. Natl. Acad. Sci. U.S.A. **106**, 4986 (2009).
[17] F. Szuecs, C. P. Kim, and W. L. Johnson, Acta Mater. **49**, 1507 (2001).
[18] D. C. Hofmann, J. Y. Suh, A. Wiest, M. L. Lind, M. D. Demetriou, and W. L. Johnson, Proc. Natl. Acad. Sci. U.S.A. **105**, 20 136 (2008).
[19] C. C. Hays, C. P. Kim, and W. L. Johnson, Phys. Rev. Lett. **84**, 2901 (2000).
[20] Y. Wang, J. Li, A. V. Hamza, and T. W. Barbee, Jr., Proc. Natl. Acad. Sci. U.S.A. **104**, 11 155 (2007).
[21] A. C. Lund and C. A. Schuh, Philos. Mag. Lett. **87**, 603 (2007).
[22] Y. Shi and M. L. Falk, Acta Mater. **56**, 995 (2008).
[23] C. A. Schuh and A. C. Lund, Nature Mater. **2**, 449 (2003).
[24] A. S. Argon, Acta Metall. **27**, 47 (1979).
[25] M. L. Falk and J. S. Langer, Phys. Rev. E **57**, 7192 (1998).
[26] E. R. Homer and C. A. Schuh, Acta Mater. **57**, 2823 (2009).
[27] L. Pechnik, Phys. Rev. E **72**, 021507 (2005).
[28] J. S. Langer, Scr. Mater. **54**, 375 (2006).
[29] E. Bouchbinder, J. S. Langer, and I. Procaccia, Phys. Rev. E **75**, 036107 (2007).
[30] J. S. Langer, Phys. Rev. E **77**, 021502 (2008).
[31] A. Minami and A. Onuki, Acta Mater. **55**, 2375 (2007).
[32] M. Tsamados, A. Tanguy, F. Leonforte, and J. L. Barrat, Eur. Phys. J. E **26**, 283 (2008).
[33] M. Tsamados, A. Tanguy, C. Goldenberg, and J. L. Barrat, Phys. Rev. E **80**, 026112 (2009).
[34] L. D. Landau and E. M. Lifshitz, *Theory of Elasticity* (Pergamon, New York, 1986), 3rd ed.
[35] W. L. Johnson and K. Samwer, Phys. Rev. Lett. **95**, 195501 (2005).
[36] $K = \mu$ implies a Poisson's ratio of $\nu = 0.125$. Our results for shear banding under simple shear are not sensitive to the choice of ν.